Paracrine interactions between epithelial cells promote colon cancer growth

Guillaume Jacquemin[1,2], Annabelle Wurmser[1], Mathilde Huyghe[1], Wenjie Sun[1], Meghan Perkins[1], Fairouz Qasrawi[1], Florent Dingli[3], Guillaume Arras[3], Damarys Loew[3] and Silvia Fre[1*]

[1]Institut Curie, Laboratory of Genetics and Developmental Biology, PSL Research University, INSERM U934, CNRS UMR3215, F-75248 Paris Cedex 05, France.

[2]Sorbonne University, UPMC University of Paris VI, F-75005, France.

[3]Institut Curie, PSL Research University, Laboratory of Mass Spectrometry and Proteomics, F-75248 Paris, France.

*Correspondence: silvia.fre@curie.fr

Abstract

Tumours are complex ecosystems composed of different types of cells that communicate and influence each other. While the critical role of stromal cells in affecting tumour growth is well established, the impact of mutant cancer cells on healthy surrounding tissues remains poorly defined. Here, we uncovered a paracrine mechanism by which intestinal cancer cells reactivate foetal and regenerative Yap-associated transcriptional programs in neighbouring wildtype epithelial cells, rendering them adapted to thrive in the tumour context. We identified the glycoprotein Thrombospondin-1 (Thbs1) as the essential factor that mediates non-cell autonomous morphological and transcriptional responses. Importantly, Thbs1 is associated with bad prognosis in several human cancers. This study reveals the Thbs1-YAP axis as the mechanistic link mediating paracrine interactions between epithelial cells, promoting tumour formation and progression.

Keywords: tumour initiation, Thrombospondin-1, YAP signalling, organoids, paracrine cell communication, colorectal cancer

Introduction

It is now well established that tumour formation and evolution are influenced by the crosstalk between cancer cells and their environment, involving complex remodelling of the extracellular matrix and interaction with stromal cells, such as cancer-associated fibroblasts, myofibroblasts, pericytes, vascular and lymphatic endothelial cells as well as different types of inflammatory immune cells[1–3]. Remodelling of the tumour microenvironment has been shown to support tumour growth through neo-angiogenesis as well as via direct effects on cancer cells exposed to pro-inflammatory and pro-survival cytokines[4]. However, tumour-stroma interactions are mostly studied among different cell types and little is known about communication between cancerous and adjacent normal epithelial cells that may contribute to tumour growth and progression. Defining the mechanisms allowing paracrine interactions between tumour and normal epithelial cells requires an understanding of how different cells persist and expand within a tumour and is crucial to dissect intratumoral heterogeneity.

We have recently reported that wildtype non-mutant intestinal stem cells can be found within intestinal tumours and contribute to tumour growth[5], suggesting the existence of bidirectional communication between tumour and normal epithelial cells. A recent study has also provided evidence that a parenchymal response of normal epithelial cells favours tumour growth and dissemination[6]. The advent of 3D organotypic cultures able to recapitulate the morphology and physiology of intestinal cells in a mesenchyme-free environment has allowed us to address the unresolved question of epithelial-specific interactions in the context of colon cancer.

Intestinal organoids are well-characterised stem-cell derived structures[7]. Importantly, organoids generated from normal intestinal crypts consistently present a stereotypical "budding" morphology, with proliferative crypts (or buds) and a differentiated villus domain. On the other hand, cells derived from intestinal tumours generally grow as hyper proliferative and non-polarised hollow spheres. The morphology of intestinal organoids directly reflects its mutational status, with wildtype cells producing budding organoids and tumour cells developing as cysts[8,9].

To study epithelial communications in a stroma-free environment, we analysed the influence of mutant organoids derived from primary mouse tumours (hereafter defined as "tumoroids") on wildtype organoids. We found that the co-culture of tumoroids and budding organoids quickly induced a hyper proliferative cystic morphology in wildtype organoids. This interaction did not require cell contact, as the effect was recapitulated by the conditioned medium from tumoroids. We found that the secreted glycoprotein Thrombospondin-1 (Thbs1) was responsible for mediating these paracrine communications, through Yap pathway activation. These studies offer novel insights into the molecular mechanisms responsible for heterogeneous tumour growth and provide an attractive therapeutic avenue in targeting Thbs1 to reduce tumour complexity.

Results

Tumour-derived epithelial cells induce a cancer-like behaviour in wildtype intestinal cells.

In an attempt to reconstitute intra-tumour heterogeneity *in vitro*, we co-cultured tumoroids from intestinal tumours derived from Apc mutant mouse[10], labelled by membrane tdTomato[11] with wildtype GFP-marked intestinal organoids, derived from lifeact-GFP mice[12] (Fig. S1A). Within 24-48 hours of co-culture with tumoroids, 5-20% of wildtype organoids, normally displaying the stereotypical budding morphology[13] (Fig. 1A), adopted an unpolarised hollow cystic shape

(indicated by arrows in Figure 1B), closely resembling the morphology of Apc mutant tumoroids[14] (Fig. 1C). To assess if this morphological change was due to mid-range paracrine or juxtacrine signals, we cultured wildtype organoids in conditioned medium (cM) from either wildtype (WT-cM) or tumour (T-cM) organoids. Consistent with our observations from co-cultures, wildtype organoids exposed to T-cM (Fig. 1E), but not to WT-cM (Fig. 1D), grew as cysts, suggesting that tumoroids secrete factors able to morphologically alter wildtype epithelial cells. Tumoroids derived from different primary tumours reproducibly induced the cystic "transformation", albeit to variable extents (Fig. S1B). The morphological change was all the more remarkable as it occurred within 6 to 12 hours of exposure to T-cM (Fig. S1C-D) and was reversed after 2-4 days, if no fresh medium was added, suggesting exhaustion of the factor(s) responsible and ruling out the possibility of acquired genetic mutations in normal organoids. Since the cystic organoid morphology has been linked to Wnt pathway activation, we analysed the expression of the quantitative Wnt reporter 7TG[15]. As shown in Figure 1F, cystic organoids grown in T-cM did not present canonical Wnt pathway activation (Fig. 1F right panel), unlike organoids stimulated with the small molecule CHIR99021, a widely used chemical Wnt activator (Fig. 1F middle panel). To further characterise the induced morphological change, we quantified the effect of T-cM on organoid proliferation and found that cystic organoids were significantly more proliferative than budding ones (compare cystic "C" and budding "B" in Fig. 1G and S1E). Indeed, while proliferative cells were restricted to the crypts in control organoids exposed to WT-cM (Fig. 1H), cystic organoids in T-cM displayed a higher proportion of undifferentiated proliferative cells, scattered throughout the newly formed cysts (Fig. 1I).

Thrombospondin-1 (Thbs1) mediates the organoid morphological and behavioural change.

Cancer cells are known to secrete numerous factors to remodel the tumour microenvironment. Having established that the morphological change was mediated by proteins present in the T-cM, since the effect was abolished upon proteinase K treatment (Fig. S2A), we performed a quantitative proteomics analysis by SILAC (Stable Isotope Labelled Amino acids in Culture) -based mass spectrometry[16] to define the composition of the T-cM relative to WT-cM. Gene Ontology analysis of the proteins over-represented in T-cM showed enrichment in cell adhesion, wound healing and generally ECM-related GO terms (Fig. S2C). We selected secreted factors that were enriched in T-cM compared to WT-cM (Fig. S2B) and explored their possible involvement in the morphological "transformation" using neutralising antibodies. Among the tested candidates, we found that neutralization of the secreted glycoprotein Thrombospondin-1 (Thbs1) alone was sufficient to entirely abolish the morphological change of wildtype organoids (Fig. 2A and S2D). Neutralization of Thbs1 with three blocking antibodies, targeting different epitopes of the protein to exclude any potential non-specific binding, was sufficient to completely block the cystic morphology (Fig. 2B, S2E). These experiments demonstrated that Thbs1 was necessary for the observed phenotype. In order to test if Thbs1 neutralization was also able to rescue the ectopic proliferation, we counted the proliferative cells per organoid. Consistent with our previous observations, T-cM-altered cystic organoids presented ectopically proliferating cells when cultured with IgG1 control antibodies (Fig. 2C-E). However, addition of anti-Thbs1 antibodies to the T-cM abolished ectopic proliferation and restricted EdU+ cells exclusively to the crypts (Fig. 2C, F). Treatment with anti-Thbs1 did not present toxicity to normal organoids, as no increase in apoptotic cells was observed (Fig. 2D-F). Moreover, Thbs1 was sufficient to induce the

morphological change, since its ectopic expression in wildtype organoids also led to cyst development (Fig. 2G-H).

Thrombospondin-1 is necessary for the growth of tumoroids but not of normal organoids.

Thbs1 is exclusively expressed by tumoroids and not by normal organoids; surprisingly, we found that Thbs1 is also essential for tumoroids growth. Indeed, neutralization of Thbs1 specifically reduced tumoroid survival and considerably arrested their growth (Fig. 3D, G-H). Importantly, the same tumoroid growth arrest was observed upon Thbs1 genetic deletion (Fig. 3F) using CRISPR-Cas9 knock-out[17]. Quantification of the proportion of dividing cells showed that, indeed, neutralization of Thbs1 significantly reduced tumoroids proliferative capacity without affecting the growth of normal organoids (Fig. 3I-N) suggesting a promising therapeutic avenue.

Wildtype organoids (re)activate a regenerative/foetal transcriptional program upon the influence of tumoroids.

In order to decipher the molecular responses of wildtype epithelial cells to T-cM, we obtained the gene expression profiles of normal organoids exposed to either T-cM or WT-cM, along with the transcriptional signature of the tumoroids from which the corresponding T-cM was derived. Interestingly, we found that differentially expressed genes in response to T-cM were enriched for genes up regulated in cancer (Fig. S3A, in bold black), including colorectal adenoma (Fig. S3A in red), suggesting that, alongside the typical tumour-like cystic morphology, wildtype cells acquire characteristics of tumour cells when exposed to T-cM. Furthermore, this analysis revealed that organoids grown in the presence of T-cM showed Yes-associated protein (YAP)/HIPPO pathway activation (Fig. S3A in green). To assess the involvement of the YAP/Hippo pathway in the

observed phenotype, we compared our RNA sequencing results to the YAP activation signature from intestinal organoids[18] using Gene Set Enrichment Analysis (GSEA), and found a strong correlation in both wildtype organoids (Fig. 4A) and tumoroids (Fig. 4D). Recent studies described YAP activation as an integral part of the regenerative and foetal programs of the normal intestinal epithelium[19]. Consistently, we found a strong correlation with the reported physiological "foetal human colitis" intestinal signature[19] (Fig. 4B, E), suggesting a link between the morphological change we characterised and reactivation of a regenerative/foetal program occurring during tumorigenesis. These findings indicate that wildtype organoids in the presence of tumour secretome switch their transcriptional program from a homeostatic to a regenerative/foetal-like response, repressing differentiation genes (Fig. 4C, F) without affecting Wnt signalling (Fig. 1F and S3B).

To assess the functional significance of YAP pathway activation, we pharmacologically blocked it using Verteporfin, an inhibitor of the YAP-TEAD interaction[20], and observed a complete loss of cystic organoids with no discernible effects on their growth (Fig. S3C-D). We further corroborated these results through the genetic deletion by CRISPR/Cas9 of Yap1 and one of its cellular effectors, the transcription factor Tead4, found up regulated upon exposure to T-cM (Fig. S3E-F). Yap1 or Tead4 knock-out in wildtype organoids (Fig. 4G) caused a considerable decrease in the proportion of cystic organoids induced by T-cM, suggesting that the YAP/Hippo pathway mediates the morphological change (Fig. 4H). We further found that wildtype organoids displayed a higher number of cells with nuclear YAP1, a readout of YAP pathway activation, upon T-cM exposure (Fig. 4I-L). However, T-cM induces nuclear YAP accumulation in both cystic and budding organoids (Fig. 4K-L), suggesting that YAP activation is necessary but not sufficient to induce the switch to the cystic phenotype.

Thbs1-expressing tumour cells can induce YAP activation in tumours *in vivo.*

In mouse tumours, we have previously characterised a population of cancer cells expressing the Notch1 receptor, which present a transcriptional signature closely related to normal intestinal stem cells and proposed that these cells could represent non-mutant epithelial cells trapped within tumours during their initial growth[5]. When we compared the expression profile of organoids grown in T-cM with the signature of Notch1-expressing intestinal tumour cells, we found a high correlation by GSEA (Fig. 5A), suggesting that wildtype cells could thrive in the tumour environment through the mechanism we have revealed in organoids exposed to T-cM. Strikingly, the Hippo signalling signature was up regulated in Notch1+ but not in Apc mutant tumour cells *in vivo* [5], corroborating the analogy between Notch1-expressing cells engulfed within tumours and organoids grown in T-cM. In mouse tumours, we found that Thbs1+ cells largely coincide with the cells expressing the widely accepted cancer stem cell marker Lgr5[21] (Fig. 5B) and do not express the differentiation marker keratin 20 (Fig. S4B). The RNA probe recognizing Thbs1 co-localize with the THBS1 protein visualized by antibody staining (Fig. S4A). Furthermore, the YAP target CTGF is expressed at high levels in cells adjacent to Thbs1+ cells (Fig. 5C). Indeed, at the whole-tumour scale, Thbs1 and CTGF expression are highly correlated (Fig. 5D, R^2=0.84). Importantly, the Thbs1-Yap axis is conserved in human cancer, as shown by the high correlation between THBS1 expression and the levels of the Yap target genes CTGF, CYR61 or WWC2 (Fig. 5G). Of further prognostic relevance, THBS1 expression is strongly correlated with poor prognosis in colon cancer (Fig. 5H), but also in kidney and gastric tumours.

Discussion

Our results indicate that in intestinal tumours derived from spontaneous Apc loss, cancer cells can directly recruit genetically wildtype epithelial cells through the secretion of the glycoprotein THBS1, which results in aberrant activation of a regenerative/foetal transcriptional program mediated by the YAP pathway (Fig. 6), a driver of intestinal regeneration and tumorigenesis[18]. THBS1 is overexpressed in a large number of solid tumours, but its role in cancer is controversial. Constitutive deletion of Thbs1 in $Apc^{Min/+}$ mice led to an increase in the number and aggressiveness of tumours, which was interpreted as a consequence of its known anti-angiogenic role[22]. However, THBS1 has been reported to promote the attachment of cells to the extracellular matrix, favouring cancer cell migration and invasion[23,24]. Indeed, a study using a model for inflammation-induced colon carcinogenesis in $Thbs1^{-/-}$ mice showed a 5-fold reduction in tumour burden, suggesting a role for THBS1 in tumour progression[25]. These contradictory results are most likely due to the multifaceted effects of THBS1, depending on which cells secrete it and which cells respond. Of interest, a recent study proposed that THBS1 induces focal adhesions (FAs) through interaction with αvβ1 integrins in the aorta[26] and FAs have been shown to directly drive YAP1 nuclear translocation in the foetal intestine[19]. Here, we found that THBS1 can "corrupt" wildtype epithelial cells in organoids, independently of stroma-derived effects allowing us to address the specific role of THBS1 on epithelial cells. Our results, corroborated by similar observations in mouse and human intestinal tumours, uncovered a novel function for this secreted multidomain glycoprotein in affecting the behaviour of normal epithelial cells surrounding a nascent tumour. Based on these results, we propose a model for tumour initiation where mutant cells can "corrupt" surrounding wildtype epithelial cells by secreting THBS1, leading to Yap activation in the receiving cells. Through the paracrine mechanism we unravelled, causing reactivation of a regenerative foetal-like

transcriptional program, wildtype epithelial cells can thrive in nascent tumours. Expansion of both mutant and wildtype cells will progressively lead to the growth of a heterogeneous tumour (Fig. 6). In such a scenario, normal cells within tumours, which would escape specific therapies targeting mutant cells, could be identified by their hallmark of Yap activation, providing a novel diagnostic tool. Of relevance, THBS1 neutralization showed a tumour-specific toxicity, offering a therapeutic target for colon cancer, potentially applicable to other epithelial tumours.

Methods

Ethics Statement

All studies and procedures involving animals were in strict accordance with the recommendations of the European Community (2010/63/UE) for the Protection of Vertebrate Animals used for Experimental and other Scientific Purposes. The project was specifically approved by the ethics committee of the Institut Curie CEEA-IC #118 and approved by the French Ministry of Research with the reference #04240.03. We comply with internationally established principles of replacement, reduction, and refinement in accordance with the Guide for the Care and Use of Laboratory Animals (NRC 2011). Husbandry, supply of animals, as well as maintenance and care of the animals in the Animal Facility of Institut Curie (facility license #C75–05–18) before and during experiments fully satisfied the animal's needs and welfare. Suffering of the animals has been kept to a minimum; no procedures inflicting pain have been performed.

Statistics and Reproducibility

Experiments were performed in biological and technical replicates as stated. For each experiment, we have used at least n=3 organoid lines originating from n=3 different mice, and experiments

with at least n=3 replicates were used to calculate the statistical value of each analysis. All graphs show mean ± SD. Statistical analysis was performed with two-tailed unpaired Welsh's t-tests, unless otherwise stated.

Transgenic mouse models

All mouse lines used have been previously described. Intestinal tumours were generated in Apc1638N mutant mice[10], crossed to the R26^{mTmG} line[11]. GFP expressing wildtype organoids were generated from the LifeAct-GFP mouse line[12]. Wildtype organoids used for KO experiments were obtained by crossing R26-LSL-Cas9-GFP[27] and R26CreERT2 mouse lines[28]. All mice used were of mixed genetic background.

Organoids cultures

Wild type organoids: Wildtype organoids were cultured and passaged as previously described [13] and derived from the intestine of 2-5 months old mice. The Matrigel-crypts mix was plated as 50 µl drops in 24-well plates or 35 µl drops in 8-well Ibidi imaging chambers (Ibidi 80827) for whole mount staining. After polymerisation the Matrigel drop was covered with wild type organoid medium containing EGF, Noggin, R-spondin1 (ENR). Reagents, media and buffers are listed in Supplementary Table S1. Factors, inhibitors and neutralising antibodies that were added to the medium are indicated in Supplementary Table S2.

Tumoroids: Apc1638N mice of more than 6 months of age were dissected and intestinal tumours were harvested using forceps and micro-dissection scissors to reduce contamination with adjacent healthy tissue. Periampullary tumours were excluded from the study to avoid contamination with

stomach cells. To remove the remaining healthy tissue surrounding the extracted tumour, tumours were incubated in 2 mM EDTA in PBS (pH=8.0) for 30 minutes at 4°C. Tumours were then briefly vortexed to detach the remaining normal tissue, leaving clean spheres. In order to dissociate tumour cells, the tumour was chopped into 1-3 mm fragments using a razor blade and digested in 66% TrypLE (Thermofischer 12605010) diluted in PBS, for 10 min at 37°C under continuous agitation at 180 RPM. The supernatant containing the dissociated cells was harvested and fresh 66% TrypLE was added to the remaining fragments for another 10 minutes. The supernatant was strained using a 70 µm cell strainer. Cells were then centrifuged at 400g for 5 minutes at 4°C, suspended in DMEM-F12 (2% Penicillin Streptomycin) and plated in 50% Matrigel drops as described for wildtype organoid cultures. After polymerisation, 300 µl of EN medium containing EGF and Noggin (EN) was added. The medium was replaced every 1-2 weeks. Tumoroids were passaged every 1 (for line expansion) or 3 to 4 weeks (for medium conditioning). Reagents, media and buffers are listed in Supplementary Table S1. The medium composition is summarised in Supplementary Table S2.

Co-culture assay

Wildtype and tumour organoid cultures were started at least two weeks before co-culture in order to use stable and exponentially growing cultures. These passages guaranteed morphologically homogeneous organoids. After passage of wildtype and tumour organoids, the fragments were mixed at approximately 3:1 wildtype organoid to tumoroids ratio. Mixed fragments were plated as described above. After Matrigel polymerisation at 37°C, 300 µl/well of ENR medium was added to allow the survival of wildtype organoids. Reagents, media and buffers are listed in Supplementary Table S1.

Conditioned medium assay

Wildtype organoids were passaged as previously described. After Matrigel polymerisation, 150 µl of ENR 2X concentrated and 150 µl of conditioned medium (cM) were added. Reagents, media and buffers are listed in Supplementary Table S1.

Tumoroid conditioned medium preparation

Established tumoroid cultures (more than two passages) were grown for 1 week. After one week of expansion, fresh medium was added and conditioned for 1 to 2 weeks depending of the organoid density. Immediately after harvesting, the conditioned medium was centrifuged at 400g for 5 minutes at 4°C to remove big debris and cell contamination. The supernatant was recovered and centrifuged again at 2.000g for 20 minutes at 4°C and then ultra-centrifuged at 200.000g for 1.5 hours at 4°C in order to remove extracellular vesicles. The supernatant was frozen in liquid nitrogen and stored at -80°C.

Wildtype conditioned medium preparation

Established wildtype organoid cultures were passaged and grown for 3 days in order to obtain high density cultures. Then, fresh ENR medium was conditioned for a maximum of 1 week and prepared as described above.

Organoid freezing

Matrigel drops containing organoids in exponential growth were collected in PBS and centrifuged twice at 400g for 5 minutes at 4°C to remove Matrigel and debris. The organoids were suspended at a high density in Cryostor10 freezing medium (six wells of organoids per 1 ml of cryogenic

medium). Organoids were incubated for 10 min in Cryostor10 before being frozen. Reagents, media and buffers are listed in Supplementary Table S1.

Organoid thawing

Organoids were quickly thawed at 37°C and suspended in 5ml of FBS prior to centrifugation at 400g for 5 minutes at 4°C. The organoids were suspended in DMEM-F12 with 2% Penicillin/Streptomycin and mixed with Matrigel at a 1:1 ratio as described above. After polymerisation at 37°C, ENR or EN medium was added. Due to the FBS impact on organoid morphology, the thawed organoids were passaged at least once and carefully checked for their morphology prior to use. Reagents, media and buffers are listed in Supplementary Table S1.

Organoid infection

Wild type or tumour organoid cultures were started at least a week before transduction. To plate 8 wells of infected organoids, 12 wells of exponentially growing organoids were harvested in cold Cell Recovery Solution and incubated on ice for 15 minutes to dissolve the Matrigel. Organoids were then centrifuged at 400g for 5 minutes at 4°C. For cell dissociation, the pellet was suspended in 2 ml of AccuMax (SIGMA A7089) containing CHIR99021, Y27632 (CY) and incubated at 37°C for 8 minutes. Digestion was then stopped by adding 2 ml of DMEM-F12 containing B27 and CY. Organoids where further mechanically dissociated by pipetting up and down 40-50 times. The cell suspension was then centrifuged at 400g for 5 minutes at 4°C. The organoids were carefully suspended in 300 µl of 66x concentrated virus (see below) containing CY and Transdux reagents prior to addition of 300 µl of cold-liquid Matrigel and plated as previously described. After polymerisation at 37°C, 300 µl/well of ENR-CY medium was added. ENR-CY was replaced

by ENR two days later. This is essential to avoid a morphological change due to exposure to CHIR99021. After 4 days, small organoids were passaged and cultured following the protocol described above. Reagents, media and buffers are listed in Supplementary Table S1.

Lentiviruses

Plasmids

Lenti-7TG was a gift from Roel Nusse (Addgene plasmid # 24314; http://n2t.net/addgene:24314; RRID: Addgene_24314). The Lenti-sgRNA-mTomato (LRT) construct was obtained by replacement of the GFP sequence with tandem Tomato in the Lenti-sgRNA-GFP (LRG), a gift from Christopher Vakoc (Addgene plasmid # 65656; http://n2t.net/addgene:65656; RRID: Addgene_65656). LentiCRISPRv2GFP was a gift from David Feldser (Addgene plasmid # 82416; http://n2t.net/addgene:82416; RRID: Addgene_82416). LentiThbs1Tg is a lentiORF expressing mouse Thbs1 (NM_011580) –myc-DKK (Origene #MR211744L3V). pMD2.G was a gift from Didier Trono (Addgene plasmid # 12259; http://n2t.net/addgene:12259; RRID: Addgene_12259). psPAX2 was a gift from Didier Trono (Addgene plasmid # 12260; http://n2t.net/addgene:12260; RRID: Addgene_12260).

sgRNA cloning

Both lentivirus backbones used for the knock-out experiments harboured the GeCKO cloning adaptors[17,29]. sgRNA inserted in either vectors are listed in Supplementary Table S3.

Virus production

Lentiviral particles were produced in HEK 293T cells. Day 0: 8 x 10^6 cells were plated onto a T75 flask in 10 ml of complete medium (see Supplementary Table S1). Day 1: cells were transfected using PEI/NaCl. For this, two solutions were prepared: mix A contained 625µl NaCl 150mM +

75µl PEI and mix B contained 625µl NaCl 150mM + 6µg of plasmid DNA at a molar ratio of 4:3:2 (lentiviral vector: psPAX2: pMD2.G). Mix A and B were incubated for 5 min at room temperature and then mixed and incubated for 15 min at RT before being added drop by drop on top of the cells. Medium was changed at day 2 and 10ml of supernatant containing virus particles was collected at day 3 and 4. The supernatants were centrifuged for 5 min at 1500rpm at 4°C in order to remove dead cells and debris. The virus particles were then concentrated to 300µl using Amicon Ultra Centrifugal Filters (UFC910024 SIGMA) by spinning at 1000g at 4°C for 1h. The virus particles were stored at -80°C.

Mass Spectrometry

Sample preparation

Isotope labelled conditioned medium requires pre-loading of isotopic amino acids in order to detect all proteins synthetized and secreted by cells[16]. To label newly produced proteins, two essentials isotopically labelled amino acids (IAA), arginine and lysine, were added to the culture medium. Wild type organoids were labelled with [$^{2}H_4$]-lysine (Lys4) and [$^{13}C_6$]-arginine (Arg6) for 2 weeks (2 passages), whilst tumoroids were labelled with [$^{13}C_6{}^{15}N_2$]-lysine (Lys8) and of [$^{13}C_6{}^{15}N_4$]-arginine (Arg10) for 2 weeks (2 passages). Then, medium was conditioned as described above using SILAC-ENR (2x1 week) or SILAC-EN (1x2weeks). After a functional assay confirming their transforming capacities, conditioned media were concentrated. Subsequently, 2 ml of tumoroids conditioned media or 4 ml of wild type conditioned media were precipitated by cold acetone. Dried protein pellets were then recovered with 50 µl of 2X Laemli buffer containing SDS and β−mercapto-ethanol (0.1%), boiled at 95°C for 5 minutes and centrifuged for 5 min at 14 000g.

MS Sample processing

Gel-based samples were cut in 8 bands and in-gel digested as described in standard protocols. Briefly, following the SDS-PAGE and washing of the excised gel slices proteins were reduced by adding 10 mM Dithiothreitol (Sigma Aldrich) prior to alkylation with 55 mM iodoacetamide (Sigma Aldrich). After washing and shrinking of the gel pieces with 100% acetonitrile, trypsin / LysC (Promega) was added and proteins were digested overnight in 25 mM ammonium bicarbonate at 30°C. Extracted peptides were dried in a vacuum concentrator at room temperature and re-dissolved in solvent A (2% MeCN, 0.3% TFA) before LC-MS/MS analysis.

LC-MS/MS analysis

Liquid chromatography (LC) was performed with an RSLCnano system (Ultimate 3000, Thermo Scientific) coupled online to an Orbitrap Fusion Tribrid mass spectrometer (MS, Thermo Scientific). Peptides were trapped on a C18 column (75 µm inner diameter × 2 cm; nanoViper Acclaim PepMapTM 100, Thermo Scientific) with buffer A' (2/98 MeCN/H2O in 0.1% formic acid) at a flow rate of 2.5 µL/min over 4 min. Separation was performed on a 50 cm x 75 µm C18 column (nanoViper Acclaim PepMapTM RSLC, 2 µm, 100Å, Thermo Scientific) regulated to a temperature of 55°C with 1) a linear gradient of 5% to 30% buffer B (100% MeCN in 0.1% formic acid) at a flow rate of 300 nL/min over 100 min. Full-scan MS was acquired in the Orbitrap analyser with a resolution set to 120,000, a mass range of m/z 400–1500 and a 4 × 105 ion count target. Tandem MS was performed by isolation at 1.6 Th with the quadrupole, HCD fragmentation with normalised collision energy of 28, and rapid scan MS analysis in the ion trap. The MS2 ion count target was set to 2 × 104 and only those precursors with charge state from 2 to 7 were sampled for MS2 acquisition. The instrument was run at maximum speed mode with 3 s cycles.

Data Processing (PRIDE and GO Analysis)

Data were acquired using the Xcalibur software (v 3.0) and the resulting spectra were interrogated by SequestHT through Thermo Scientific Proteome Discoverer (v 2.1) with the Mus musculus Swissprot database (022017 containing 16837 sequences and 244 common contaminants). The mass tolerances in MS and MS/MS were set to 10 ppm and 0.6 Da, respectively. We set carbamidomethyl cysteine, oxidation of methionine, N-terminal acetylation, heavy $^{13}C_6{}^{15}N_2$-Lysine (Lys8) and $^{13}C_6{}^{15}N_4$-Arginine (Arg10) and medium $^{2}H_4$-Lysine (Lys4) and $^{13}C_6$-Arginine (Arg6) as variable modifications. We set specificity of Trypsin digestion and allowed two missed cleavage sites. The resulting files were further processed by using myProMS (v 3.5)[30]. The SequestHT target and decoy search results were validated at 1% false discovery rate (FDR) with Percolator. For SILAC-based protein quantification, peptides XICs (Extracted Ion Chromatograms) were retrieved from Thermo Scientific Proteome Discoverer. Global MAD normalization was applied on the total signal to correct the XICs for each biological replicate (n=3). Protein ratios were computed as the geometrical mean of related peptides. To estimate ratio significance, a t-test was performed with the R package limma[31] and the false discovery rate was controlled using the Benjamini-Hochberg procedure[32] with a threshold set to 0.05. Proteins with at least two peptides, a 2-fold enrichment and an adjusted p-value < 0.05 were considered significantly enriched in sample comparisons.

Pathway enrichment

Gene ontology (GO) terms enrichment analysis used the proteins significantly enriched in sample comparisons (T-cM/WT-cM; 2peptides, fold change >2, adjusted p-value<0.05) and the unique proteins to T-cM. GO biological processes, cellular components, and molecular functions were

analysed using the UniProt-GOA Mouse file (v. 20181203). We defined the significant GO with the criterion of p-value < 0.05.

Immunofluorescence (IF)

For whole mount IF, organoids were grown on 8well-chamber slides (Ibidi 80827). For EDU staining, EDU was added 2h before starting the immunofluorescence procedure at a concentration of 10µM (Carbosynth Limited NE08701). After fixation using 4% Paraformaldehyde (Euromedex 15710) in PBS for 1h at room temperature, organoids were washed with PBS and permeabilised in PBS + 1% triton X-100 (Euromedex 2000-C) for 1h at room temperature. Organoids were then incubated with 150µl of diluted antibodies (see Supplementary Table S4) in blocking buffer (PBS, 2% BSA, 5% FBS, 0.3% Triton X-100) overnight at room temperature. After 3 washes of 5 min in PBS, 150µl of secondary antibodies were added together with DAPI diluted in PBS and incubated at room temperature for 5h. Organoids were then washed with PBS for 3 times for 5 min each and stored in 1:1 ratio PBS and glycerol (Euromedex 15710) before imaging. For EDU staining, EDU signal was revealed after the secondary antibody step, using the EDU click-it kit according to the manufacturer's protocol (Thermofisher scientific C10340).

RNA single molecule Fluorescence In Situ Hybridization (RNA-smFISH)

RNA-smFISH analyses were performed using RNAscope® Multiplex Fluorescent Detection Kit v2 kit (ACD 323110) and pipeline following manufacturer's recommendations. Thbs1 mRNA were labelled using RNAscope® Probe- Mm-Thbs1-C3 (#457891-C3), CTGF mRNA were labelled using RNAscope® Probe- Mm-CTGF (#314541) and Lgr5 mRNA were labelled using RNAscope® Probe- Mm-Lgr5 (#312171). In order to subsequently perform immunostaining after

RNAScope FISH, protease III step has been performed and should not exceed 20 minutes. Subsequent antibody staining was performed as described.

Epithelial masks generation

To quantify RNAscope results only in epithelial cells, epithelial masks were generated using E-cadherin immunostaining. After Ilastik training allowing segmentation of E-cadherin-stained membranes, masks were smoothed by closing function (iteration=15) and holes filling. Generated masks were manually checked for consistency.

smFISH dots quantification

Raw images were segmented using Ilastik (v1.3.2) and training on negative controls (background), positive controls and experimental slides (dots). Segmented masks were cleaned using FIJI through an opening function, 2px Gaussian blur and Moments threshold. Generated masks were manually checked for consistency with raw data. Aggregates of dots were partially rescued using watershed function and dots (size=2-250 circularity=0.50-1.00) analysed using build-in Analyse Particle function. Epithelial dots were obtained by multiplication of dot masks by the corresponding epithelial masks previously generated.

Image acquisition

Images were obtained on an Inverted Wide Confocal Spinning Disk microscope (Leica) using 40x/1.3 OIL DIC H/N2 PL FLUOR or 20x/0.75 Multi immersion DIC N2 objectives and Hamamtsu Orca Flash 4.0 camera. Images were captured using Metamorph. Whole plate acquisition was performed using a dissecting microscope and Cell Discoverer 7 (Leica). Images

were captured using ZEN. For RNAscope experiments, images were obtained on PLAN APO 40x/1.3NA o objective on an upright spinning disk (CSU-X1 scan-head from Yokogawa) microscope (Carl Zeiss, Roper Scientific France), equipped with a CoolSnap HQ2 CCD camera (Photometrics). Images were captured using Metamorph.

Nuclear/cytoplasmic YAP1 quantification

Nuclear IF ratios were obtained using a custom-made ImageJ macro. This macro segmented the nuclei on the DAPI channel using Otsu Threshold, Watershed and Particles analysis. For each segmented nucleus, a cytoplasmic halo of 8 pixels was generated and excluded from the DAPI mask to avoid false cytoplasmic measure in neighbouring nuclei. The mean intensities of the segmented nucleus and cytoplasmic regions of interest (nROI and cROI) were then measured in the IF channel (nIF and cIF). Cells were counted only if: area ratio nucleus/cytoplasm > 0.5, avoiding bias of pixel sampling either due to miss-segmentation or to overcrowded regions. Results (nIF, cIF and ratio) were then processed on Microsoft Excel. A density curve of the nIF / cIF ratio was performed for each category of organoid in order to observe peaks trends of positive and negative nuclei for IF. Threshold was defined manually in the inter-peak region. To avoid interpretation of low and uncertain signal, a minimal mean intensity cut-off for cIF was picked from pictures. Using the threshold and the cut-off, the percentage of nIF^{HIGH} cells per organoid was calculated.

RNA-sequencing

Sample preparation

Organoids were harvested using Cell recovery solution as described above. After 15 minutes of Matrigel dissolution, organoids were pelleted at 500g for 5 minutes. Pellets were recovered in 1ml

of PBS in 1.5ml tubes and pelleted again at same conditions. RNA extraction was performed using RNEasy Mini Kit (Qiagen) following manufacturer's recommendations. Total RNA integrity (RINe) were subjected to quality control and quantification using an Agilent TapeStation instrument showing excellent integrity (RNA Integration Number, RIN=10). Nanodrop spectrophotometer was used to assess purity based on absorbance ratios (260/280 and 260/230).

RNA Sequencing

RNA sequencing libraries were prepared from 1µg of total RNA using the Illumina TruSeq Stranded mRNA Library preparation kit which allows to prepare libraries for strand specific mRNA sequencing. A first step of polyA selection using magnetic beads was performed to address sequencing specifically on polyadenylated transcripts. After fragmentation, cDNA synthesis was performed followed by dA-tailing before ligation of the TruSeq indexed adapters (Unique Dual Indexing strategy). PCR amplification was finally achieved to create the final cDNA library. After qPCR quantification, sequencing was carried out using 2x100 cycles (paired-end reads, 100 nucleotides) on an Illumina NovaSeq 6000 system (S1 flow cells) to get around 45M paired-end reads per sample. Fastq files were generated from raw sequencing data using bcl2fastq where demultiplexing was performed according to indexes.

RNA-seq data processing

Sequencing reads were aligned on the Mouse reference genome (mm10) using the STAR mapper (v2.5.3a) [33]. Protein-coding genes from the Gencode annotation (vM13) have been used to generate the raw count table. Overall sequencing quality controls report a very high sequencing quality, a high fraction of mapped reads, and a high enrichment in exonic reads.

Differential analysis

Expressed genes (TPM>=1 in at least one sample) have then been selected for supervised analysis. The raw count table was normalised using the TMM method from the edgeR R package (v3.25.9)[34], and the limma[31] voom (v3.39.19) functions were applied to detect genes with differential expression. In order to compare tumoroids versus wiltype samples, we design a linear model as follow:

$$Y_{its} = \mu_i + T_{it} + E_{it}$$

where T is the type effect (T={WT-cM, T-cM, Tumoroids}). We then restricted the dataset to WT-cM and T-cM samples, and applied the following model:

$$Y_{its} = \mu_i + T_{it} + S_s + E_{its}$$

where T is the type effect (T={WT-cM, T-cM}) and S is the sample effect (S={sample1, sample2, sample3}). All raw p-values were corrected for multiple testing using the Benjamini-Hochberg (BH) method. Genes with an adjusted pvalue <0.05 and a log2 fold-change >1 were called significant.

Pathway enrichment

We applied the pathway enrichment on the up-regulated genes (pvalue < 0.05 and logFC > 1) in T-cM and tumoroids versus to normal organoids by using KEGG, MSigDB curated gene sets and MSigDB regulatory target gene sets. The enrichment analysis was performed by R package clusterProfiler (v3.14.3) and msigdbr (v7.1.1).

Source code is available at this address:

https://gist.github.com/wenjie1991/d79fe428ac80c8f2e5d781a966df3978

Gene set enrichment analysis

GSEA v4.0.3 was used to generate and calculate the enrichment score. Transcriptional signatures used for the analysis were extracted from the literature[5,18,19,35] and Nusse Lab (https://web.stanford.edu/group/nusselab/cgi-bin/wnt/target_genes). GSEA were calculated by gene set and 1000 permutations in our RNASeq normalised reads count matrix.

Clinical colon cancer gene expression analysis

The gene expression data and clinical variables from the TCGA Colon Adenoma (COAD) cohort were downloaded from TSVdb[36] on 20th Jun 2020. Analyses were performed on Primary Solid Tumour gene expression data subset. Pairwise correlation analysis assayed THBS1, CTGF, CYR61 and WWC2 on 285 COAD tumour samples. The expression data were transformed by log2. Then, the Spearman correlation was calculated and visualized by the PerformanceAnalytics (v2.0.4) R package. In the survival analysis, 268 COAD tumour samples with overall survival follow-up information were used. The original data time scale in days was converted to years (365 days per year) and analysed up to 5 years. We defined the samples with upper one-third THBS1 expression as "THBS1 high group" and rests as "THBS1 low group". Log-rank test and Kaplan Meier graph were obtained using the R package survminer (v0.4.7).

Source code is available at this address:

https://gist.github.com/wenjie1991/6ff60b3edd5f61d0bd2ebe4f9404e46e

References

1. Marusyk, A. *et al.* Non-cell-autonomous driving of tumour growth supports sub-clonal heterogeneity. *Nature* **514**, 54–58 (2014).
2. Cleary, A. S., Leonard, T. L., Gestl, S. A. & Gunther, E. J. Tumour cell heterogeneity maintained by cooperating subclones in Wnt-driven mammary cancers. *Nature* **508**, 113–117 (2014).
3. Hanahan, D. & Coussens, L. M. Accessories to the Crime: Functions of Cells Recruited to the Tumor Microenvironment. *Cancer Cell* **21**, 309–322 (2012).
4. Balkwill, F. R., Capasso, M. & Hagemann, T. The tumor microenvironment at a glance. *J. Cell. Sci.* **125**, 5591–5596 (2012).
5. Mourao, L. *et al.* Lineage tracing of Notch1-expressing cells in intestinal tumours reveals a distinct population of cancer stem cells. *Sci Rep* **9**, 888 (2019).
6. Ombrato, L. *et al.* Metastatic-niche labelling reveals parenchymal cells with stem features. *Nature* **572**, 603–608 (2019).
7. Sato, T. & Clevers, H. Growing Self-Organizing Mini-Guts from a Single Intestinal Stem Cell: Mechanism and Applications. *Science* **340**, 1190–1194 (2013).
8. Drost, J. *et al.* Sequential cancer mutations in cultured human intestinal stem cells. *Nature* **521**, 43–47 (2015).
9. Sato, T. *et al.* Long-term expansion of epithelial organoids from human colon, adenoma, adenocarcinoma, and Barrett's epithelium. *Gastroenterology* **141**, 1762–1772 (2011).
10. Fodde, R. *et al.* A targeted chain-termination mutation in the mouse Apc gene results in multiple intestinal tumors. *Proc. Natl. Acad. Sci. U.S.A.* **91**, 8969–8973 (1994).

11. Muzumdar, M. D., Tasic, B., Miyamichi, K., Li, L. & Luo, L. A global double-fluorescent Cre reporter mouse. *Genesis* **45**, 593–605 (2007).
12. Riedl, J. *et al.* Lifeact: a versatile marker to visualize F-actin. *Nat. Methods* **5**, 605–607 (2008).
13. Sato, T. *et al.* Single Lgr5 stem cells build crypt-villus structures in vitro without a mesenchymal niche. *Nature* **459**, 262–265 (2009).
14. Schwank, G. *et al.* Functional repair of CFTR by CRISPR/Cas9 in intestinal stem cell organoids of cystic fibrosis patients. *Cell Stem Cell* **13**, 653–658 (2013).
15. Brugmann, S. A. *et al.* Wnt signaling mediates regional specification in the vertebrate face. *Development* **134**, 3283–3295 (2007).
16. Ong, S.-E. *et al.* Stable Isotope Labeling by Amino Acids in Cell Culture, SILAC, as a Simple and Accurate Approach to Expression Proteomics. *Mol Cell Proteomics* **1**, 376–386 (2002).
17. Shalem, O. *et al.* Genome-Scale CRISPR-Cas9 Knockout Screening in Human Cells. *Science* **343**, 84–87 (2014).
18. Gregorieff, A., Liu, Y., Inanlou, M. R., Khomchuk, Y. & Wrana, J. L. Yap-dependent reprogramming of Lgr5(+) stem cells drives intestinal regeneration and cancer. *Nature* **526**, 715–718 (2015).
19. Yui, S. *et al.* YAP/TAZ-Dependent Reprogramming of Colonic Epithelium Links ECM Remodeling to Tissue Regeneration. *Cell Stem Cell* **22**, 35-49.e7 (2018).
20. Liu-Chittenden, Y. *et al.* Genetic and pharmacological disruption of the TEAD-YAP complex suppresses the oncogenic activity of YAP. *Genes & Development* **26**, 1300–1305 (2012).
21. Barker, N. *et al.* Crypt stem cells as the cells-of-origin of intestinal cancer. *Nature* **457**, 608–611 (2009).

22. Gutierrez, L. S., Suckow, M., Lawler, J., Ploplis, V. A. & Castellino, F. J. Thrombospondin 1--a regulator of adenoma growth and carcinoma progression in the APC(Min/+) mouse model. *Carcinogenesis* **24**, 199–207 (2003).
23. Sid, B. *et al.* Thrombospondin-1 enhances human thyroid carcinoma cell invasion through urokinase activity. *Int. J. Biochem. Cell Biol.* **40**, 1890–1900 (2008).
24. Tuszynski, G. P., Gasic, T. B., Rothman, V. L., Knudsen, K. A. & Gasic, G. J. Thrombospondin, a potentiator of tumor cell metastasis. *Cancer Res.* **47**, 4130–4133 (1987).
25. Lopez-Dee, Z. P. *et al.* Thrombospondin-1 in a Murine Model of Colorectal Carcinogenesis. *PLoS ONE* **10**, e0139918 (2015).
26. Yamashiro, Y. *et al. Matrix mechanotransduction mediated by thrombospondin-1/integrin/YAP signaling pathway in the remodeling of blood vessels*. http://biorxiv.org/lookup/doi/10.1101/814533 (2019) doi:10.1101/814533.
27. Platt, R. J. *et al.* CRISPR-Cas9 knockin mice for genome editing and cancer modeling. *Cell* **159**, 440–455 (2014).
28. Ventura, A. *et al.* Restoration of p53 function leads to tumour regression in vivo. *Nature* **445**, 661–665 (2007).
29. Sanjana, N. E., Shalem, O. & Zhang, F. Improved vectors and genome-wide libraries for CRISPR screening. *Nat. Methods* **11**, 783–784 (2014).
30. Poullet, P., Carpentier, S. & Barillot, E. myProMS, a web server for management and validation of mass spectrometry-based proteomic data. *Proteomics* **7**, 2553–2556 (2007).
31. Ritchie, M. E. *et al.* limma powers differential expression analyses for RNA-sequencing and microarray studies. *Nucleic Acids Res.* **43**, e47 (2015).

32. Benjamini, Y. & Hochberg, Y. Controlling the False Discovery Rate: A Practical and Powerful Approach to Multiple Testing. *Journal of the Royal Statistical Society. Series B (Methodological)* **57**, 289–300 (1995).
33. Dobin, A. *et al.* STAR: ultrafast universal RNA-seq aligner. *Bioinformatics* **29**, 15–21 (2013).
34. Robinson, M. D., McCarthy, D. J. & Smyth, G. K. edgeR: a Bioconductor package for differential expression analysis of digital gene expression data. *Bioinformatics* **26**, 139–140 (2010).
35. Merlos-Suárez, A. *et al.* The Intestinal Stem Cell Signature Identifies Colorectal Cancer Stem Cells and Predicts Disease Relapse. *Cell Stem Cell* **8**, 511–524 (2011).
36. Sun, W. *et al.* TSVdb: a web-tool for TCGA splicing variants analysis. *BMC Genomics* **19**, 405 (2018).
37. Perez-Riverol, Y. *et al.* The PRIDE database and related tools and resources in 2019: improving support for quantification data. *Nucleic Acids Res.* **47**, D442–D450 (2019).

Acknowledgments

We are very grateful to Prof. Shahragim Tajbakhsh for the mTmG reporter line and to Dr. Danijela Vignjevic for sharing the lifeACT-GFP reporter mouse. We are also grateful to Dr. Jean-Leon Maitre, Dr. Raphael Margueron and their team members for technical advice and constructive discussions. We would like to acknowledge the PICT-IBiSA imaging platform and the Flow Cytometry and Cell Sorting Platform at Institute Curie for their expertise; the In Vivo Experimental Facility, mainly Sonia Jannet, for help in the maintenance and care of our mouse colony as well as the NGS platform of Institut Curie for RNA sequencing and Dr. Nicolas Servant for bioinformatics support. **Funding:** This work was supported by Paris Sciences et Lettres (PSL*

Research University) (grant # C19-64-2019-228), the French National Research Agency (ANR) grant number ANR-15-CE13-0013-01, the Canceropole Ile-de-France (grant # 2015-2-APD-01-ICR-1), the Ligue contre la cancer (grant #RS19/75-101) and by Labex DEEP ANR-Number 11-LBX-0044 to SF. GJ was funded by a PSL PhD fellowship and the French Association for Cancer Research (ARC # DOC20180507411). The Laboratory of Mass Spectrometry and Proteomics was supported by grants from Région Île-de-France (2013-2EML-02-ICR-1, 2014-2-INV-04-ICR-1) and FRM (DGE20121125630). The PICT-IBiSA imaging platform was funded by ANR-10-INBS-04 (France-BioImaging), ANR-11 BSV2 012 01, ERC ZEBRATECTUM N°311159, ARC SFI20121205686 and from the Schlumberger Foundation. The ICGex NGS platform of the Institut Curie was supported by the grants ANR-10-EQPX-03 (Equipex) and ANR-10-INBS-09-08 (France Génomique Consortium) from the Agence Nationale de la Recherche ("Investissements d'Avenir" program), by the Canceropole Ile-de-France and by the SiRIC-Curie program - SiRIC Grant INCa-DGOS- 4654.

The funders had no role in study design, data collection and analysis, decision to publish, or preparation of the manuscript.

Author contributions: Guillaume Jacquemin [Conceptualisation, Data curation, Formal Analysis, Funding acquisition, Investigation, Methodology, Validation, Visualisation, Writing – original draft, Writing – review & editing]; Annabelle Wurmser [Investigation]; Mathilde Huyghe [Investigation, Validation, Visualisation]; Wenjie Sun [Data curation, Formal Analysis]; Meghan Perkins [Investigation]; Fairouz Qasrawi [Investigation]; Florent Dingli [Investigation, Methodology]; Guillaume Arras [Data curation, Formal Analysis]; Damarys Loew [Project

administration, Formal Analysis]; Silvia Fre [Conceptualisation, Funding acquisition, Project administration, Resources, Supervision, Writing – original draft, Writing – review & editing].

Competing interests: the authors declare no competing interests.

Materials & Correspondence: further information and requests for resources and reagents should be directed to and will be fulfilled by the corresponding author Silvia Fre (silvia.fre@curie.fr)

Data and materials availability: The mass spectrometry proteomics data have been deposited to the ProteomeXchange Consortium via the PRIDE partner repository with the dataset identifier PXD020002[37]. The RNA sequencing data have been deposited in the Gene Expression Omnibus (GEO) repository under accession code GSE153160: Whole-genome transcriptomic analysis of intestinal organoids and tumoroids. All other data supporting the conclusions of this study are provided in the main text or the supplementary materials.

Jacquemin et al. Figure 1

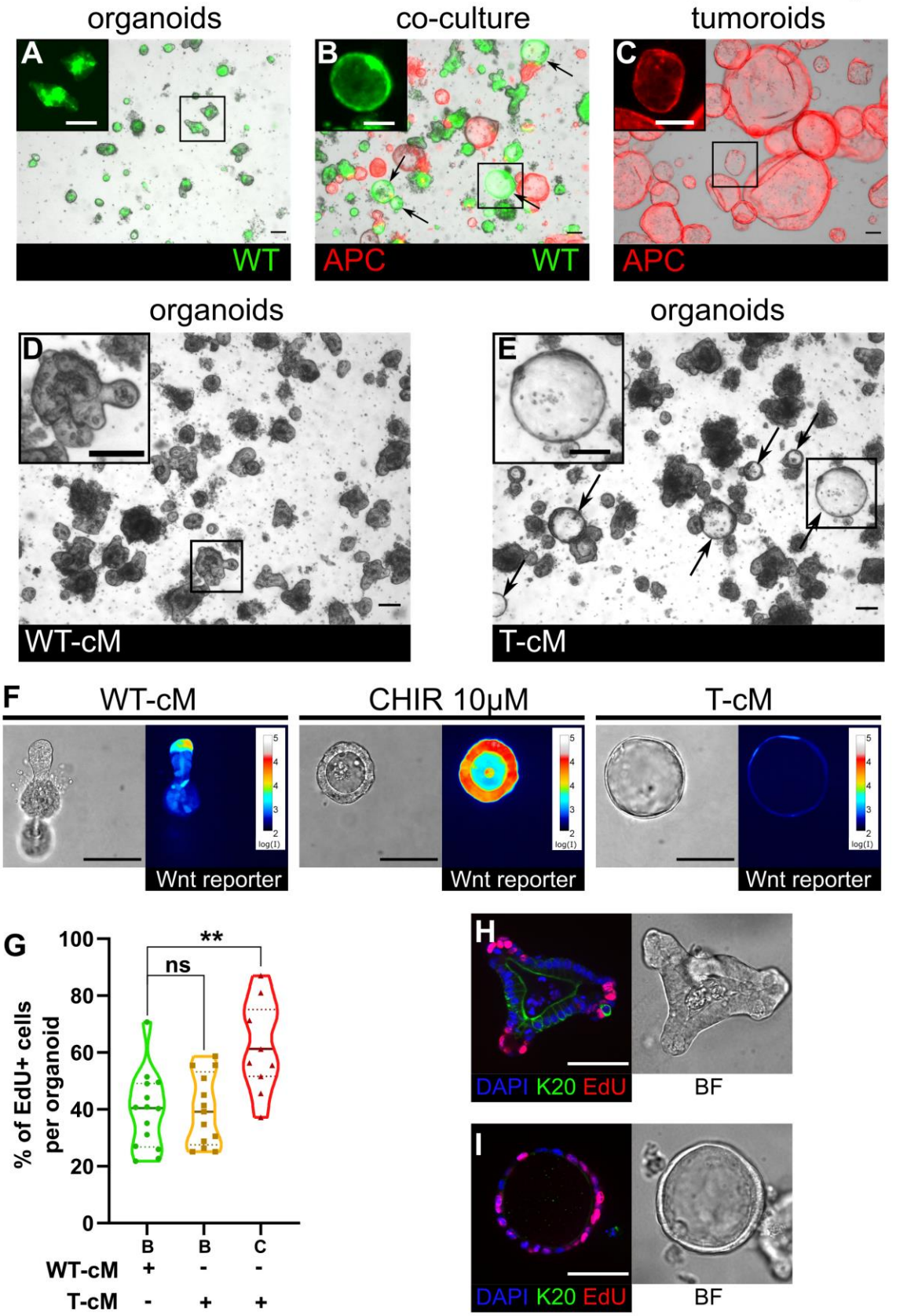

Fig. 1. Tumoroids secrete soluble factors that induce a tumour-like cystic morphology in wildtype organoids. (A) Wildtype budding organoids marked by lifeact-GFP (in green) after 24h in culture. (B) Wildtype organoids marked by lifeact-GFP after 24h in co-culture with tdTomato-expressing tumoroids. Arrows indicate green cystic organoids. (C) APC mutant tumoroids marked by tdTomato after 24h in culture. (D-E) Wildtype budding organoids exposed to conditioned medium from wildtype organoids (WT-cM in D) or from tumoroids (T-cM in E). Arrows indicate cystic organoids in E. (F) Representative organoids expressing the Wnt reporter 7TG exposed to WT-cM, 10µM CHIR99021 (CHIR 10 µM) or T-cM for 24h. Pseudo-colour shows log10 intensities of the reporter fluorescence. (G) Quantification of the percentage of EdU+ cells per organoid for budding organoids grown in WT-cM (B – WT-cM, n=14), budding organoids grown in T-cM (B – T-cM, n=13) or cystic organoids grown in T-cM (C – T-cM, n=9). (H-I) Immunofluorescence for proliferative cells (EdU in red) and differentiated cells (anti-K20 in green) in wildtype organoids grown in WT-cM (H) or in T-cM (I). The corresponding bright field images (BF) are shown in the right panels. DAPI stains DNA in blue. Scale bar = 100µm.

**: pvalue < 0.01

Jacquemin et al. Figure 2

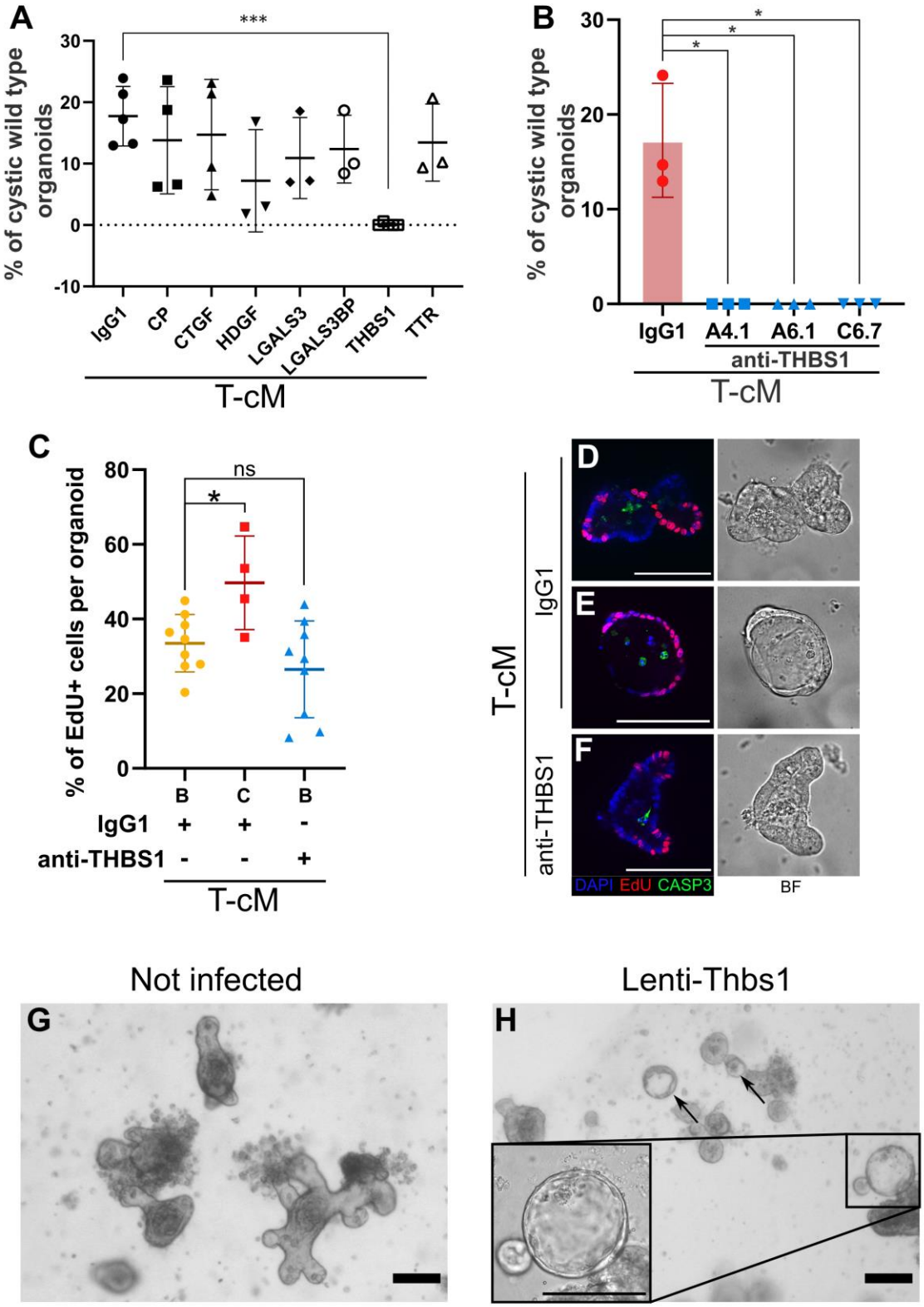

1

Fig. 2. Thrombospondin-1 is necessary for the morphological "transformation" of wildtype organoids. (A) Quantification of the percentage of wildtype cystic organoids in T-cM upon neutralization with blocking antibodies against Ceruloplasmin (CP), Connective tissue growth factor (CTGF), Hepatoma derived growth factor (HDGF), Galectin-3 (LGALS3), Galectin-3 binding protein (LGALS3BP), Thrombospondin-1 (THBS1), Transthyretin (TTR) (5 µg/ml). (B) Quantification of the percentage of wildtype cystic organoids in T-cM upon neutralization with three different blocking antibodies against THBS1 (clones A4.1, A6.1 and C6.7 at 5 µg/ml). (C) Quantification of the percentage of EdU+ cells (2h pulse) per organoid for wildtype budding (B – IgG1, n=9) or cystic organoids (C – IgG1, n=4) exposed to T-cM in the presence of IgG1 or antibodies anti-THBS1 (B – anti-THBS1, n=9). (D-F) Whole-mount immunostaining for proliferation (EdU in red) and apoptosis (anti-cleaved CASP3 in green) of wild type organoids exposed to T-cM with anti-IgG1 (D-E) or anti-THBS1 (F). DAPI stains DNA in blue. The corresponding bright field (BF) images are shown on the right panels. (G-H) Representative pictures of self-transformed wild type organoids overexpressing Thbs1 (Lenti-Thbs1 in H) and not infected organoids (G). Black arrows indicate cystic wildtype organoids in H. Scale bar = 100µm. *: pvalue < 0.05; ***: pvalue < 0.001. Graphs indicate average values ± SD.

Jacquemin et al. Figure 3

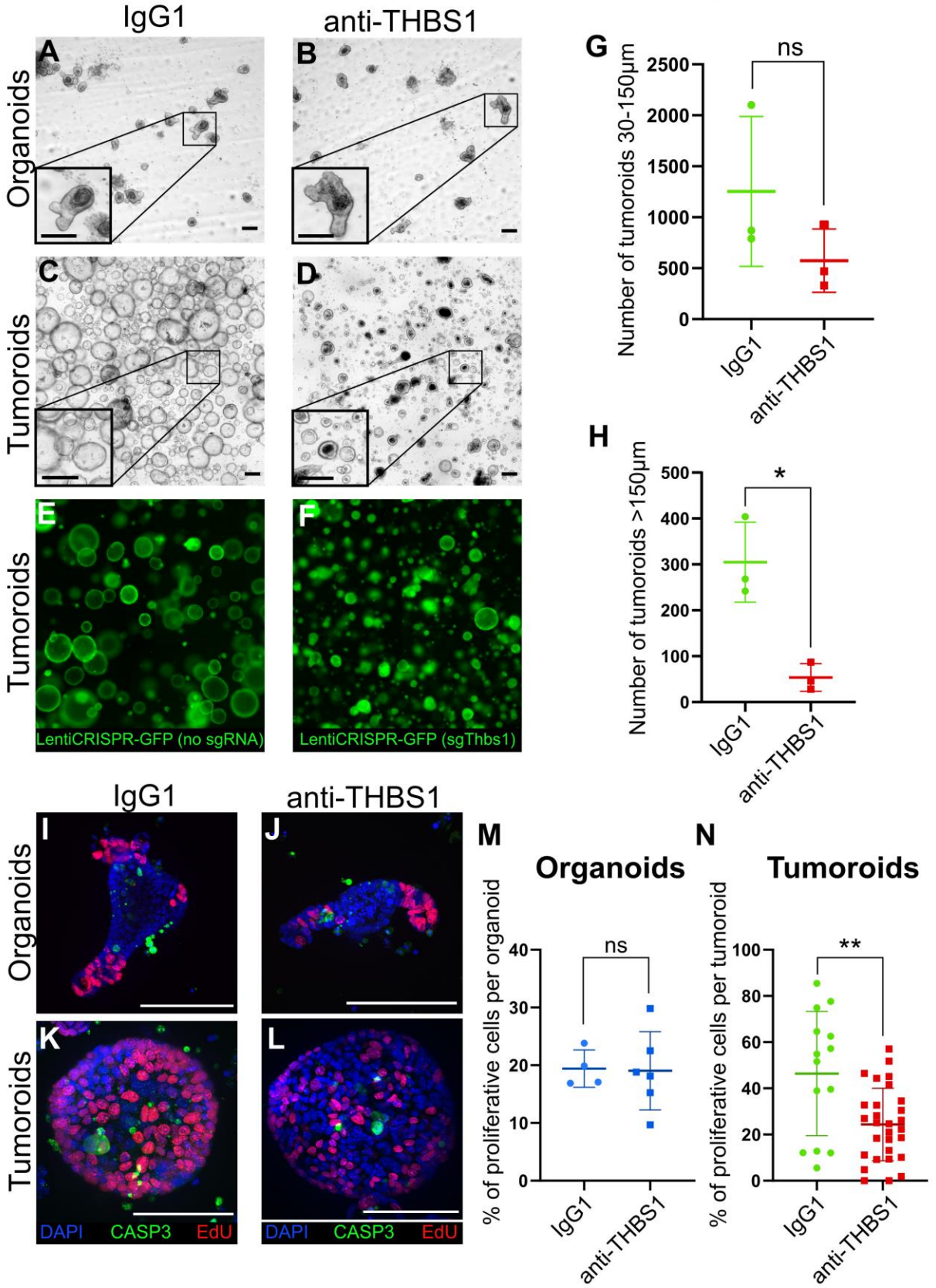

1

Fig. 3. Thrombospondin-1 is necessary for the growth of tumoroids. (A-D) Representative bright field images of wildtype organoids (A-B) or tumoroids (C-D) incubated with IgG1 isotype control antibodies (A and C) or anti-THBS1 A6.1 neutralising antibody (B and D) (10 µg/ml). (E-F) Representative images of tumoroids infected with LentiCRISPR-GFP without sgRNA (E) or targeting Thbs1 (sgThbs1 in F). (G-H) Quantification of the number of tumoroids upon antibody neutralization relative to their size: small tumoroids between 30 to 150µm in G; large tumoroids of more than 150 µm diameter in H. (I-L) Immunofluorescence of proliferative cells (EdU in red) and apoptosis (anti-cleaved Caspase-3 CASP3 in green) of wildtype organoids (I-J) or tumoroids (K-L) exposed to IgG1 isotype control antibodies (I and K) or to anti-THBS1 A6.1 neutralising antibody (J and L). Quantification of EdU+ cells per organoid (M) or tumoroid (N) in the presence of IgG1 or anti-THBS1 A6.1. Graphs indicate average values ± SD.

Jacquemin et al. Figure 4

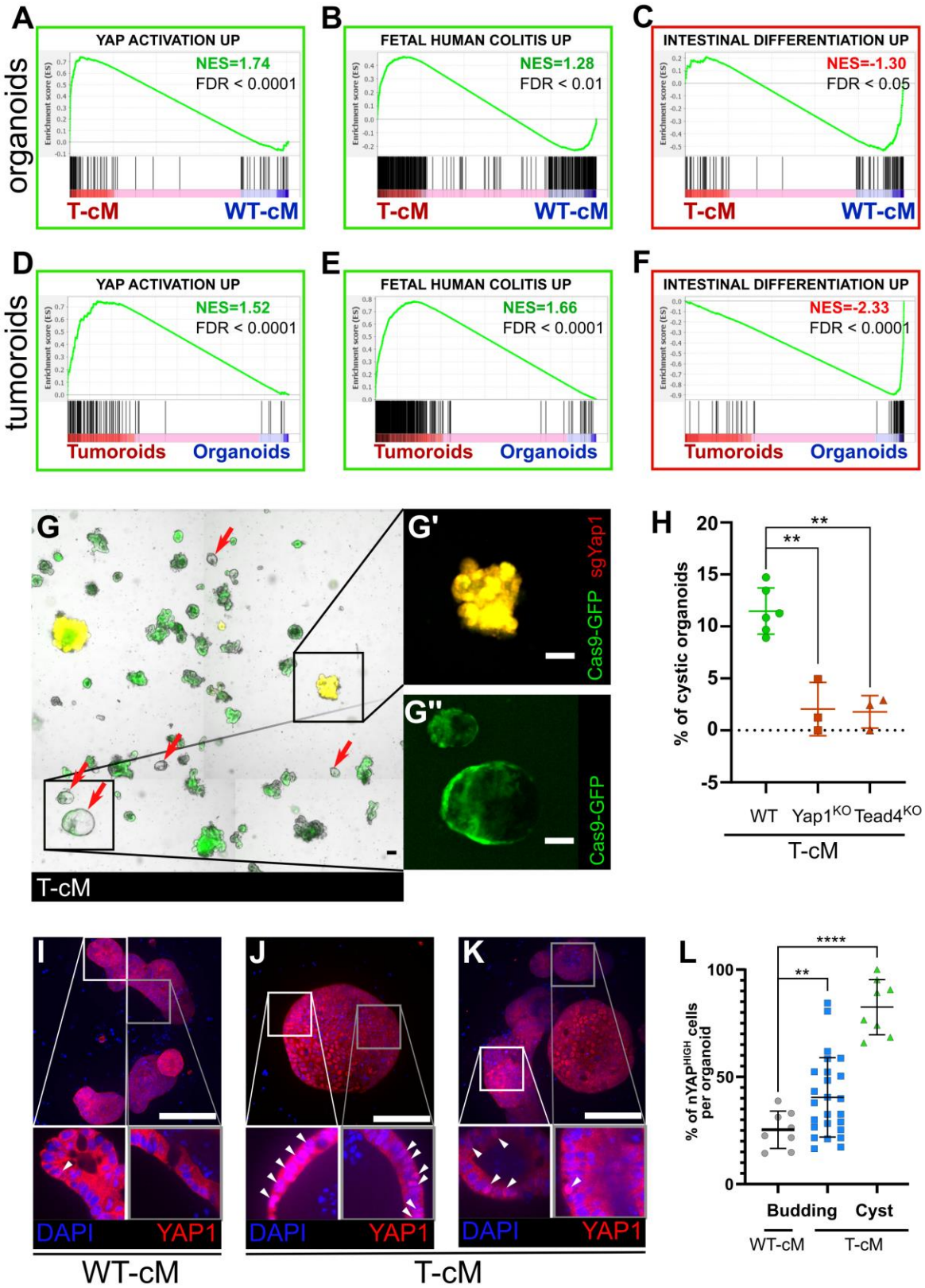

1

Fig. 4. T-cM induces YAP pathway activation and a foetal-like lineage reversion in wild type organoids. Gene Set Enrichment Analyses (GSEA) showing the correlation between the transcriptional changes induced in wildtype organoids by T-cM (A-C) or in tumoroids (D-F) and the indicated transcriptional signatures. NES: Normalised Enrichment Score; green NES = positive correlation; red NES = inverse correlation. (G) Representative image of organoids expressing Cas9-GFP (in green) transduced with a sgRNA targeting Yap1 (sgYap1 in red). Higher magnification of a budding $Yap1^{KO}$ organoid (in yellow in G') and a cystic $Yap1^{WT}$ organoid expressing only Cas9-GFP (in green in G''). (H) Percentage of cystic organoids induced by exposure to T-cM in organoids WT, $Yap1^{KO}$ or $Tead4^{KO}$, as indicated. (I-K) Max projection of immunostaining for YAP1 (in red) of wild type organoids exposed to WT-cM (I), or T-cM (J-K) presenting cystic (J) or budding (K) morphologies. DAPI stains DNA in blue. White arrowheads pinpoint YAP^{HIGH} cells in Z-section insets. (L) Quantification of the percentage of YAP^{HIGH} cells/organoid based on the ratio of nuclear vs. cytoplasmic YAP1 in cystic and budding wild type organoids grown in WT-cM or T-cM. Scale bars correspond to 100µm in G, I, J, K. **: pvalue < 0.01; ****: pvalue < 0.0001. Graphs indicate average values ± SD.

Jacquemin et al. Figure 5

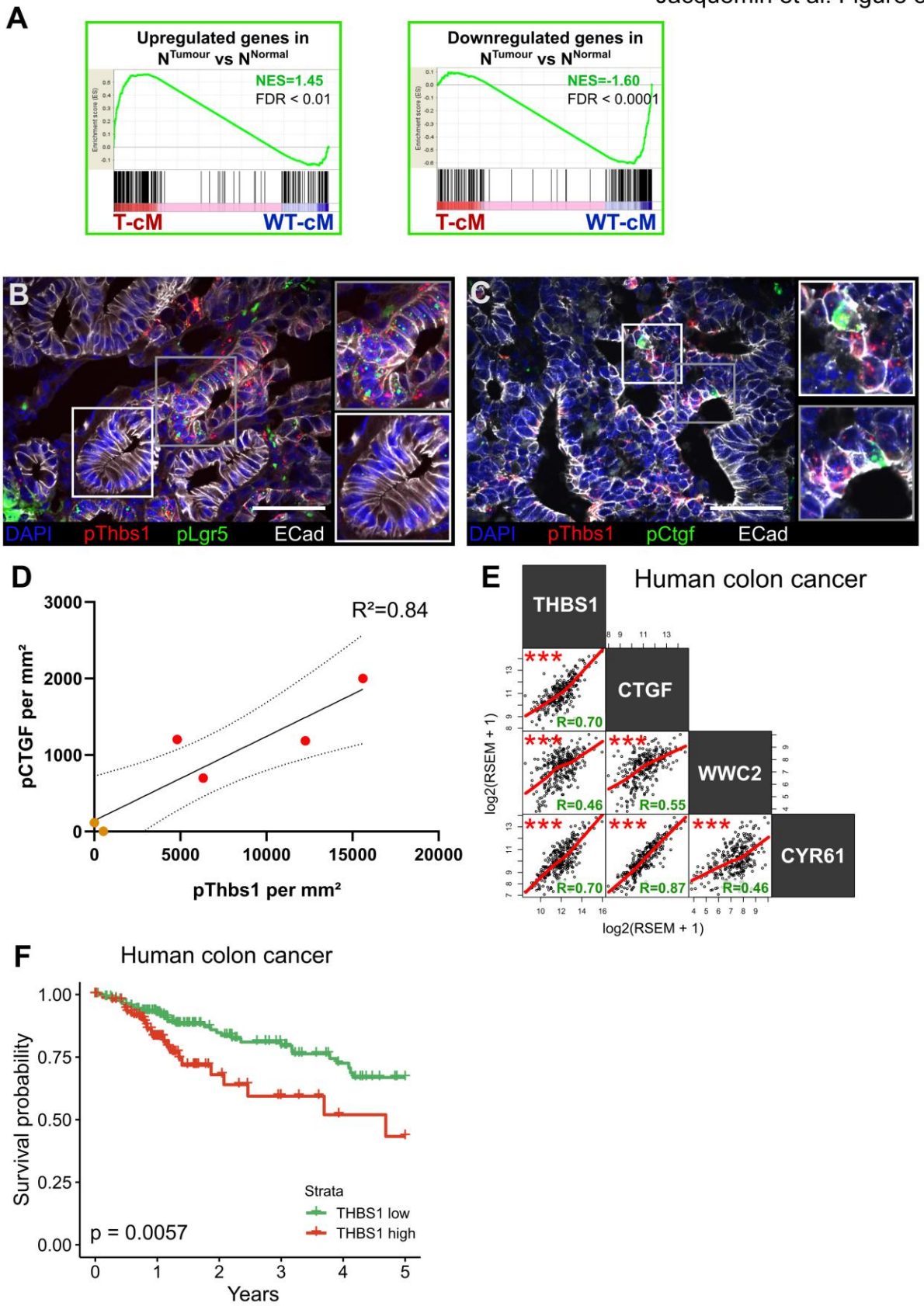

1

Fig. 5. Thbs1 is expressed by Lgr5+ cancer stem cells in vivo and induces YAP activation in neighbouring epithelial cells. (A) Gene Set Enrichment Analyses (GSEA) showing the correlation between the transcriptional changes induced in wildtype organoids by T-cM and differentially expressed genes in Notch1-expressing intestinal tumour cells compared to normal stem cells (green NES = positive correlation). (B-C) Representative sections of Apc mutant intestinal tumours analysed by smFISH for Lgr5 (green in B) or CTGF (green in C) and Thbs1 (red) and immune-stained with anti-E-cadherin antibody (white) to demarcate epithelial cells. DAPI labels nuclei in blue. (D) Correlation of the number of RNA dots/mm² for the CTGF and Thbs1 probes in mouse intestinal tumours. Red samples indicate large tumours (≥8mm), orange samples were small tumours (<8mm). Dashed lines indicate 95% confidence intervals. (E) Correlation matrix between the expression of Thbs1 and the indicated Hippo signalling targets in human primary tumours from the TCGA colon cancer datasets. R indicates the Spearman coefficient. (F) Overall survival of colon cancer patients stratified into THBS1 high (red) and low (green) groups by a threshold of the top one-third quantile of THBS1 expression. ***: pvalue < 0.001.

Jacquemin et al. Figure 6

A In organoids

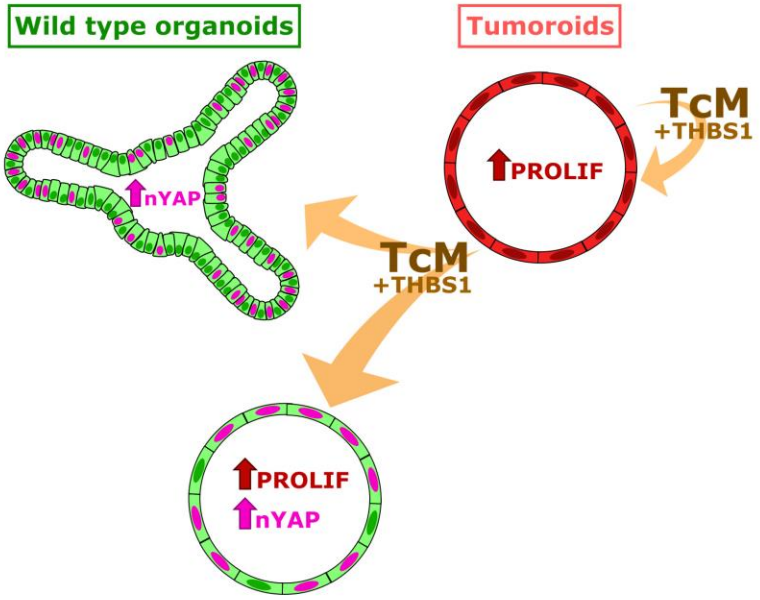

B In vivo

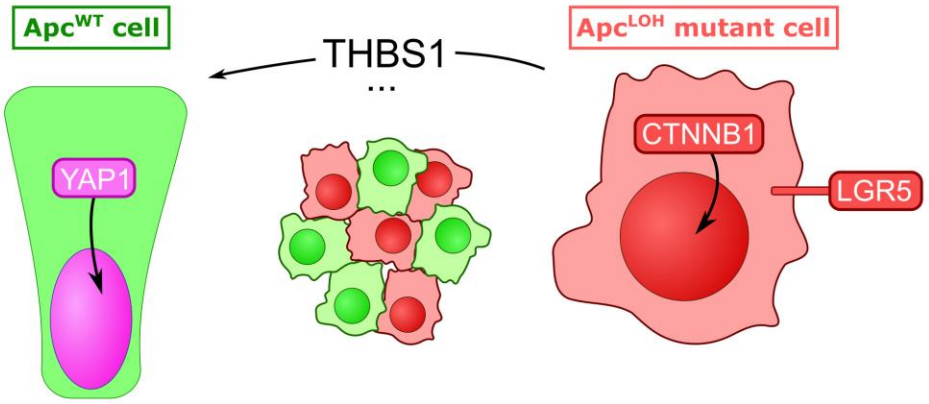

1

Fig. 6. Model for epithelial cell interactions in tumours. (A) In stroma-free organoids, mutant tumoroids "corrupt" genetically wildtype organoids by secreting Thrombospondin-1 (orange arrows). This results in YAP1 nuclear translocation (drawn as pink nuclei) and hyper proliferation upon cystic "transformation". (B) In tumours, mutant tumour cells (Apc^{LOH}) secrete THBS1 at the early stages of tumour onset. THBS1, through YAP pathway activation, confers a tumour-like behaviour to wildtype cells present in the tumour environment, thereby generating intratumoral cell heterogeneity.